



RESEARCH ARTICLE OPEN ACCESS

Hybrid Radial-Axial Flow for Enhanced Thermal Performance in Packed Bed Energy Storage

Mohammad M. S. Al-Azawii¹  | Ryan Anderson^{2,3} 

¹Department of Mechanical Engineering, University of Misan, Amarah, Misan, Iraq | ²Energy Research Institute, Montana State University, Bozeman, Montana, USA | ³Chemical and Biological Engineering, Montana State University, Bozeman, Montana, USA

Correspondence: Mohammad M. S. Al-Azawii (mohammed.alazawii@uomisan.edu.iq) | Ryan Anderson (ryan.anderson@montana.edu)

Received: 1 May 2024 | **Revised:** 10 September 2024 | **Accepted:** 11 September 2024

Funding: The authors received no specific funding for this work.

Keywords: charging efficiency | hybrid radial-axial (HRA) flow | packed bed TES | thermal energy storage

ABSTRACT

In this work, a hybrid radial-axial (HRA) system is used to store thermal energy in a packed bed. The heat transfer fluid (HTF) is delivered via a perforated radial pipe placed at the center of the packed bed along the axial length. Hot fluid flows from the center toward the wall through the holes (like other radial systems), but then leaves via the traditional axial flow exit, creating the HRA flow configuration. A computational fluid dynamics (CFD) model is used to analyze the thermal performance of the packed bed during the charging process utilizing the new HRA system. Alumina beads of 6 mm were filler materials and air was HTF with inlet temperature of 75°C for proof of concept. The present paper focuses on two aims: (1) utilizing CFD models to analyze flow and temperature profiles in the packed bed; (2) comparing the model results to experimental results published in a previous HRA flow study and to traditional axial flow. Two HRA configurations were considered based on previous experimental designs, one with uniform holes in the central pipe (R_1) and one with gradients in the hole sizes to promote even flow from the central pipe into the bed (R_2). The numerical results agree with the experimental results in both cases. The HRA system performance depends on the flow profile created by the hole designs, and it can perform better than the axial flow depending on the design of the radial pipe. Design R_2 , which promotes even flow from the central pipe into the bed, has higher charging efficiency than standard axial flow methods. For HRA design R_2 at 0.0048 m³/s (7 SCFM, standard cubic feet per minute), numerical results for charging efficiency were 75.5% versus 73.8% for traditional axial flow. For HRA design R_2 at 0.0061 m³/s (9 SCFM), numerical charging efficiency was 80.5% versus 78.1% for traditional axial flow. These results are consistent with experimental data.

1 | Introduction

Thermal energy storage (TES) technology can integrate with renewable energy sources such as solar to provide continuous power from concentrated solar power plants [1] or can be utilized to capture and store industrial waste heat [2]. Packed beds are a potential TES storage system, and traditional designs use axial flow of the heat transfer fluid through the bed. In the axial configuration, flow goes from one end to the other (i.e., z -direction flow), and the flow direction reverses between charging and discharging. Several reviews have

focused on the performance and design of traditional axial flow systems [3, 4].

Radial flow TES is a new technique to store energy in the packed bed by charging/discharging the bed domain radially, along the r -direction of the cylinder [5]. Currently, few studies have used radial flow to store/recover thermal energy in packed bed storage systems. Charging the bed radially reduces the flow's length scale and thus reduces thermal dispersion losses [6], leading to improved energetic efficiencies, and it can also lower the pressure drop compared with a traditional axial

This is an open access article under the terms of the [Creative Commons Attribution-NonCommercial-NoDerivs](https://creativecommons.org/licenses/by-nc-nd/4.0/) License, which permits use and distribution in any medium, provided the original work is properly cited, the use is non-commercial and no modifications or adaptations are made.

© 2024 The Author(s). *Energy Storage* published by John Wiley & Sons Ltd.

flow system. McTigue and White [7] numerically studied radial flow TES and compared the results to axial flow behavior. For that design, radial flow improved performance in terms of pressure drop but decreased thermal performance due to increased losses to the environment. Trevisan et al. [8] investigated radial flow with high temperature TES with two perforated pipes serving as boundaries in a cylindrical packed bed of natural rocks. During the charging processes, hot gas entered the large-diameter inner pipe from the vessel's top and flowed radially through the packing material. After depositing the energy, the air left the packed bed from the bottom through the outer pipe. During the discharging processes, the flow direction reversed. Results showed a 46% reduction in radiation thermal losses and a 50% reduction in pressure losses compared with traditional axial flow storage tanks. Recently, Trevisan et al. [9, 10] introduced a novel radial storage packed bed using an inward radial HTF flow during the charging process and reversed fluid flow during the discharging process. The study showed a reduction in thermal and pressure losses. Gerstle et al. [11] studied a $100\text{kWh}_{\text{th}}$ radial TES packed bed experimentally and numerically, where air and pea gravel were used as HTF and storage materials, respectively. The study showed an exergetic recovery efficiency of about 90%. Another innovative radial system, THERMS, was proposed by Ho and Gerstle [12]. Their analysis showed leveled costs of storage of $\$0.04/\text{kWh}_e$ and $\$0.13/\text{kWh}_e$ depending on duration (short term vs. long-term). Skuntz et al. [13] analyzed the influence of aspect ratio on TES system efficiency with radial and axial flow. The results showed that pressure drop for radial flow was lower than that in axial flow for certain aspect ratios. However, the highest net efficiency, including pressure drop and thermal performance, from axial flow was higher than in radial flow. Recently, Anderson et al. [14] numerically investigated a radial flow system with segmentation, where the bed domain was divided into several zones and each zone was charged/discharged independently. Like other studies, flow moved unidirectionally in the radial direction. In the segmented design, the thermal performance was higher than axial flow, but the pressure drop was too high to be used in practical application.

Most radial flow systems consider low aspect ratios, where the vessel diameter is large. In these cases, the central and receiving pipes are also large diameter, which promotes even flow distribution of HTF into/from the packing domain. While that is a benefit, it leads to a larger system volume overall, and not all the volume is storage volume since the large inner and outer pipes cannot store energy. In contrast, Beck et al. [15] investigated even flow distribution in the packed bed domain using radial flow where the container has a high aspect ratio ($L > D$). A high aspect ratio strongly influences the thermal performance as uneven flow can occur from the central pipe to the packed bed. Their results showed that varying the hole size in the center pipe along the length of the central pipe can promote more uniform flow into the bed. When the hole sizes were the same, flow would typically go to the end of the center pipe before entering the packing, effectively bypassing the packing domain. Smaller holes at the outlet of the center pipe led to more flow resistance in those zones, promoting more uniform flow into the bed from the holes throughout the central pipe. Flow uniformity into a packed bed via a radial pipe was also analyzed by [16].

As noted, these emerging systems using radial flow all considered fluid moving from the center to the wall or the wall to the center with no axial flow within the packed bed [5, 7–15]. However, in our previous work [17] a novel method was used to charge the bed with flow that moved radially and axially in the bed by inserting a perforated radial pipe along the length of the bed domain. Flow exits the center pipe radially, and then flows to the traditional axial outlet, which is termed hybrid radial-axial (HRA) charging. In HRA, there is no radial receiving pipe near the wall as is done in purely radial-based systems and the central pipe is a relatively narrow diameter, keeping system volume smaller than other radial systems. In the previous HRA experiments, the thermal behavior during the charging process was analyzed for six different central pipe designs and compared with that of traditional axial flow. The results showed that the hole size and hole size distribution of the perforations influenced flow uniformity into the bed. When the central pipe was designed correctly, hybrid flow was more efficient than axial flow in terms of charging efficiency. However, the study was achieved experimentally, and no additional details were available about transport within the porous domain.

To the best of the author's knowledge, no other TES systems using radial pipe injection for HRA flow have been considered in the literature. In this work, the unique HRA packed bed TES system is analyzed numerically during the charging process. Specific objectives are to analyze the velocity profiles and movement of the thermal front in the bed over time to explain why the charging efficiency is enhanced with certain designs. These objectives are met with a computational fluid dynamics (CFD) model in COMSOL Multiphysics to simulate the flow and thermal behavior inside the storage packed bed, providing insights not possible with experiments alone. The heat transfer model results focus on temperature profiles, velocity profiles, total energy in the bed, and charging efficiency. Designs R_1 and R_2 in the present study are modeled, which represent Designs A and E of our previous study [17], where the geometry, radial pipe designs, layers, and dimensions of the radial holes/layers were explained in detail. These designs were chosen because they had two different perforation patterns in the central pipe that strongly affected flow into the bed. In these cases, R_1 was an initial design that did not perform well energetically, while R_2 's design led to better thermal performance during charging. Air was used as HTF at 75°C , and alumina with $d_p = 6\text{ mm}$ was used as storage materials. Both designs are studied at two air flow rates, and the results of the HRA configurations are compared with traditional axial flow at the same charging conditions. Design R_2 shows better performance than axial flow methods based on the stored energy and thermal efficiency during the charging process.

2 | System Design, Modeling Approach, Energy, and Efficiency Analysis

2.1 | Design of the Radial Pipe

The dimensions of the central radial pipe are shown in Table 1, where two designs are modeled and analyzed. R_1 has a constant hole size and R_2 segments the pipe into four zones of equal length but with different hole sizes. As discussed, smaller holes

toward the outlet promote even flow from the central pipe into the packed bed. The diameters of these holes ranged from 1.58 to 3.18 mm. The piping system is 100 cm long with perforations created by drilling four holes at 1 cm intervals. Each subsequent set of four holes is rotated 45° around the pipe.

2.2 | CFD Modeling: Temperature and Velocity Profiles

The geometry of the problem approximates a lab-scale apparatus whose experimental results are utilized in this work is shown in Figure 1. As can be seen, the flow inlet is into the central pipe. Fluid moves along the center pipe and through the radial holes, shown in the inset, into the packed bed. The fluid exits the packing material at the outlet of the bed and is collected by additional piping downstream (piping not shown). This combination of flow entering a central pipe but exiting via the packing domain at the other end is the HRA concept. In Figure 1a, the inset also shows how there are four holes at each axial drill

TABLE 1 | Dimensions of the central radial pipe holes, number of holes in each layer, and length of layers for designs R₁ and R₂ (A and E in the previous study [17]).

Design/pattern	Length of layers (cm)	Hole diameter (in) mm
R ₁	L	100 (3/32) 2.38
R ₂	L1	25 (3/32) 2.38
	L2	25 (1/8) 3.18
	L3	25 (3/32) 2.38
	L4	25 (1/16) 1.58

Note: More details about the design of the radial pipes and schematic of the storage packed bed can be found in [17].

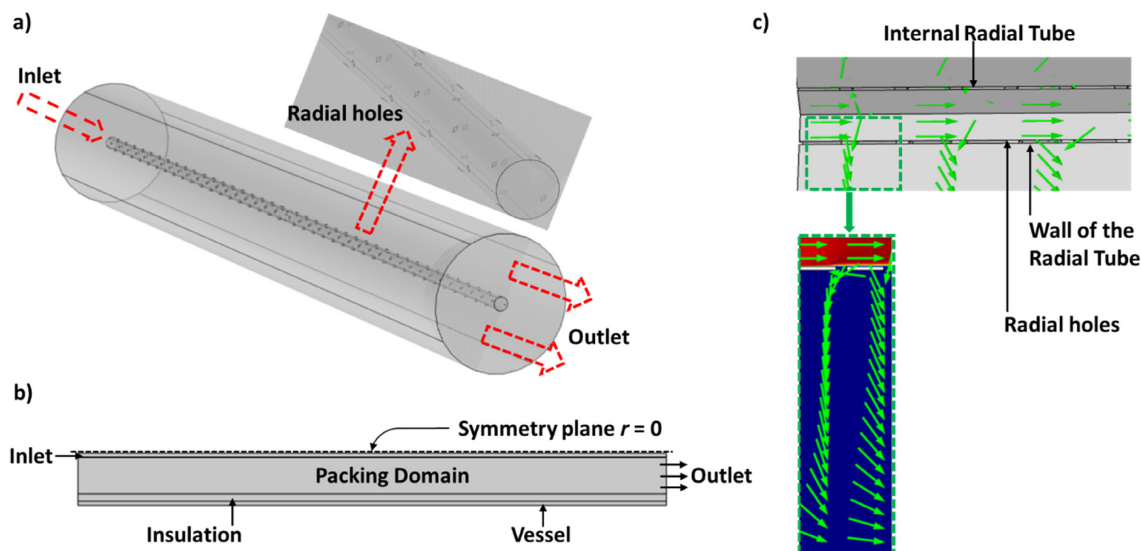


FIGURE 1 | (a) The experimental geometry of the cylindrical storage packed bed with central pipe in 3-D for design R₂. Perforations in the central pipe allow for air flow from the central pipe to the packing domain. (b) Schematic of the 2-D axisymmetric modeling approach used in this work. Fluid enters the central pipe at the inlet and exits the system via the packed bed outlet as occurs in 3-D. (c) Flow profile for HRA. Fluid in the center internal pipe is in the axial (z) direction. Air flows through the holes in the central pipe in the radial (r) direction. Once in the packed bed, the flow profile has radial and axial directions of flow.

location as explained above. However, modeling this 3D domain is computationally demanding and thus the model was solved in a two-dimensional axisymmetric approach, shown in Figure 1b. To ensure this simplification is appropriate, flow from a full 3D model was compared with flow results in the 2D axisymmetric model (results not shown). Flow profiles were assessed at the inlet, middle, and outlet of the packing domain, and agreement was noted between the magnitude of the velocity and the overall flow direction (e.g., more pronounced radial toward the inlet while fully axial toward the outlet). Figure 1c shows the HRA system in the 2D axisymmetric model. Air flows axially in the central pipe and exits the holes in the radial direction. Once in the packed bed, the velocity vectors indicate spatially variable radial and axial flow.

The packed bed measures 1 m in length and 16.8 cm in diameter, with 1.27 cm of insulation inside a 0.3556 cm thick steel vessel. The central pipe is 0.953 cm inner diameter with a wall thickness of 0.158 cm. The central pipe was built using array, difference, and union functions to define the dimensions of each hole, the number of holes, and the space between the holes.

In solving the model, flow through the central pipe, holes, and packed bed is modeled first independent of the heat transfer. The resulting velocity profile from the radial holes is then used in the heat transfer model as a boundary condition for the flow. The flow exiting these holes enters the packed bed, where both flow and heat transfer are considered. Considering the modest inlet temperature in this system and thus limited variation in the HTF's thermophysical properties, this is an acceptable simplification.

COMSOL Multiphysics 6.1 was used to solve the governing equations. In the flow only model, Equations (1–3) were solved for mass conservation, momentum conservation in the central pipe, and momentum conservation in the packed bed. The Ergun equation solves for pressure in the packed bed [18].

$$\frac{\partial \rho}{\partial t} + \nabla \cdot (\rho \mathbf{u}) = 0 \quad (1)$$

$$\frac{\rho \partial \mathbf{u}}{\partial t} + \rho (\mathbf{u} \cdot \nabla) \mathbf{u} = \nabla \cdot [-p\mathbf{I} + \mu(\nabla \mathbf{u} + (\nabla \mathbf{u})^T)] \quad (2)$$

In the packed bed domain, the equation of momentum is:

$$\frac{\rho}{\varepsilon} \frac{\partial \mathbf{u}}{\partial t} + \frac{\rho}{\varepsilon} (\mathbf{u} \cdot \nabla) \frac{\mathbf{u}}{\varepsilon} = \nabla \cdot \left[-p\mathbf{I} + \frac{\mu}{\varepsilon} (\nabla \mathbf{u} + (\nabla \mathbf{u})^T) - \frac{2\mu}{3\varepsilon} (\nabla \cdot \mathbf{u})\mathbf{I} \right] - (\mu K^{-1} + \beta |\mathbf{u}|) \mathbf{u} \quad (3)$$

where, \mathbf{u} is the velocity vector, ρ is the gas density, μ is the gas viscosity, and p is the pressure, K is the permeability associated with viscous losses, and β is a coefficient for the inertial losses in the packed bed. The permeability, K (m^2) and Forchheimer coefficient, β (kg/m^4), represent the porous viscous and inertial losses, respectively and are calculated from the Ergun equation assuming a porosity of $\varepsilon = 0.375$ and a particle size $d_p = 6$ mm.

In a separate model, the heat transfer in porous media physics is used to determine the temperature distribution in all domains with the 2-D axisymmetric model. The temperature is determined in all four regions defined in the model: fluid, porous domain, insulation, and steel. The general governing equations are adopted from [15]. A single-phase energy equation modeled the heat transfer in porous media, where the fluid and solid are assumed in local thermal equilibrium ($T_f = T_s = T$) [18]. This approach has been used successfully in our previous work [19–21] with an air-alumina packed bed storage system. The single-phase equation assumes a homogenous medium [22] and uses effective properties for the volumetric heat capacity and thermal conductivity based on a weighted average of the amount of solid and fluid in the bed as determined by the porosity.

$$(\rho C_p)_{\text{eff}} \frac{\partial T}{\partial t} + (\rho C_p)_f \mathbf{u} \cdot \nabla T = \nabla \cdot (k_{\text{eff}} \nabla T) + Q_{\text{loss}} \quad (4)$$

The equation for the solid domains (insulation and steel domains) is:

$$(\rho C_p)_i \frac{\partial T}{\partial t} = \nabla \cdot (k_i \nabla T) \quad (5)$$

where the subscript i denotes either the insulation or steel vessel. Q_{loss} represents heat loss to the environment via natural convection from the vessel walls. The wall heat transfer coefficient used in the model is $3.67 \text{ W}/\text{m}^2\text{K}$ based on typical wall temperatures and heat transfer correlations [23]. Thermophysical properties of the various components are given in Table 2.

TABLE 2 | Thermophysical properties of all solid materials and HTF.

	Alumina	Steel	Insulation	Pipe	Air
k (W/mK)	26.8	20	0.025	0.18	0.033
ρ (kg/m^3)	3982	7850	300	1190	1.009
c_p (J/kgK)	920.9	485	1050	1470	1009

The boundary and initial conditions used in the model efforts during the charging process are: $T_{t=0} = 20^\circ \text{C}$, $T_{\text{inlet}} = 75^\circ \text{C}$, $\dot{m}_{t=0} = 0$, $\dot{m}_{\text{inlet}} = 0.0040$ and $0.0050 \text{ kg}/\text{s}$. In the previous study [17], one flow rate of $0.0048 \text{ m}^3/\text{s}$ (7 SCFM) was used to analyze the thermal performance due to the radial flow during the charging period. In the present study, two flow rates were chosen: A flow rate of $0.0048 \text{ m}^3/\text{s}$ (7 SCFM) was chosen for consistency with previous experimental results and a flow of $0.0061 \text{ m}^3/\text{s}$ (9 SCFM) was analyzed numerically and experimentally as well. The mesh size used in the model was fine (free Triangular) with maximum and minimum element sizes equal to 0.053 and 0.0003 m . The results as a function of mesh were checked, and the change in results was small and could be neglected.

2.3 | Energy and Efficiency Analysis

Based on the first law of thermodynamics (steady-flow thermal energy equation) [24], Equation (6) determines the energy stored in the bed domain.

$$Q_{\text{bed}} = \int_{T_o}^{T_{\text{bed}}} m C_{p_{\text{alumina}}}(T) dT \quad (6)$$

where, T_o and T_{bed} are the initial and averaged bed temperature, m is the mass of alumina, and $C_{p_{\text{alumina}}}$ is the heat capacity of the alumina beads, which is determined as a function of temperature from Reference [20]. The total energy delivered to the system is defined in Equation (7):

$$Q_{\text{supplied}} = \dot{m} C_{p_{\text{air}}} \int_0^{t_s} (T_{\text{hot}} - T_o) dt \quad (7)$$

where, \dot{m} is the mass flow rate, $C_{p_{\text{air}}}$ is the specific heat capacity of the air (constant here), T_{hot} is the inlet temperature ($T_{\text{hot}} = 75^\circ \text{C}$), T_o is the ambient temperature, and t_s is the storage time.

Equation (8) calculates the charging efficiency, which is the ratio of energy stored in the bed to energy supplied to the storage bed.

$$\zeta_{\text{charging}} = \frac{Q_{\text{bed}}}{Q_{\text{supplied}}} \quad (8)$$

The charge time is a function of alumina properties and the flow rate of the HTF as shown in [20]. The resulting charge times are approximately 6540 and 5100s for 0.0048 and $0.0061 \text{ m}^3/\text{s}$, respectively, for HRA charging. These durations, along with the volume-average temperature in the bed at the end of charging, are used in Equations (6) and (7) to determine the efficiency.

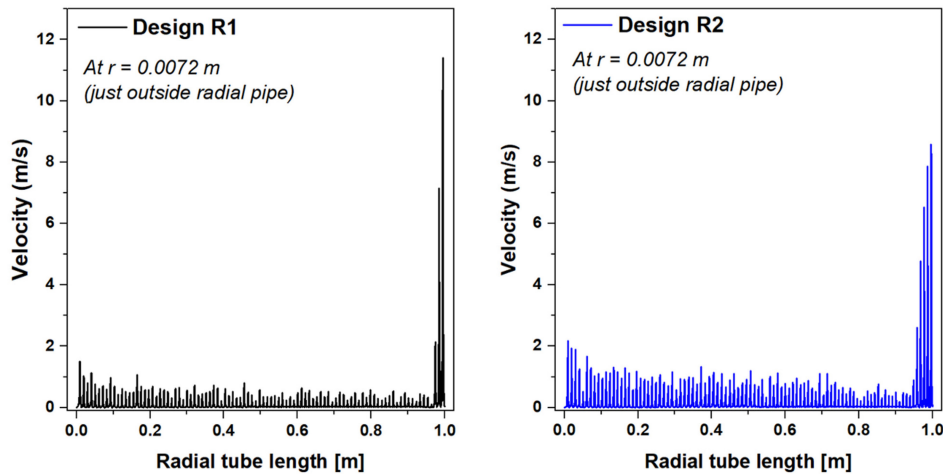


FIGURE 2 | Flow velocity at $r=0.0072$ m, located near the radial pipe perforations for design R_1 and R_2 . Design R_2 lessens bypass flow toward the exit and promotes even flow into the bed along the length of the radial pipe, which enhances performance during charging.

3 | Results and Discussion

The results focus on flow distribution from the radial pipe into the packed bed and the resulting temperature distributions over time. Charging efficiency and energy stored are also analyzed for these two HRA designs along with a traditional axial flow configuration.

3.1 | Thermal Performance: Velocity and Temperature Profiles

For velocity profiles, flow at $0.0048 \text{ m}^3/\text{s}$ was chosen to analyze the velocity impacts for designs R_1 and R_2 based on the results from the numerical model. At a flow rate of $0.0061 \text{ m}^3/\text{s}$, the same trend is noticed. Figure 2 shows the strong influence that the radial pipe design has on the flow into the packed bed (flow only model). These results show the velocity magnitude just outside the radial pipe at $r=0.0072$ m. The jaggedness of the profiles is from the flow exiting discrete openings along the radial pipe length from 0 to 1 m. Compared with design R_2 , design R_1 results in a lower velocity along much of the bed from 0 to ~ 0.95 m and then displays a much higher velocity toward the end of the radial pipe. This means the constant hole diameter in design R_1 promotes flow bypass where heated flow would not enter as much of the bed. As will be shown, this effect lowers the charging efficiency. Based on these results, average velocities were used as boundary conditions at the holes into the bed in the heat transfer model.

Versus a unique velocity in each of the 100 holes, these results informed different velocities that could be used as approximations for several holes. In design R_1 , 10 average velocities were used, and in design R_2 , 14 average velocities were used to capture the oscillations in velocity seen in both profiles. Including more or fewer averages did not strongly affect the heat transfer results.

Figure 3 shows the resulting flow in the heat transfer model based on averaging the velocity exiting the perforations at three axial locations (inlet, middle, and outlet) for design R_2 .

As can be seen at the inlet, the flow is radial from the central pipe toward the wall of the bed. As expected, the magnitude of the radial flow velocity decreases from the center to the wall in the packed bed domain. Further from the inlet and closer to the wall, the hot gas flows axially. At the center of the bed, the flow is both radial and axial. Again, flow near the wall is more axial than radial at the wall versus the center of the bed. Finally, the flow is predominantly in the axial direction at the outlet of the bed. Flow from the inlet region to outlet region also shows the magnitude of the velocity increases from inlet to outlet. This behavior is expected for HRA flow since flow exiting any of the holes along the central pipe must exit at the common outlet.

The temperature distribution from the model is compared with the temperature distribution from the experimental results for two flow rates 0.0048 and $0.0061 \text{ m}^3/\text{s}$. Figures 4 and 5 show the temperature profiles inside the bed domain along the axial length for designs R_1 and R_2 , respectively at $r=3.8$ cm (the radial location of two thermocouples in the experimental study) [17]. As can be seen, the model results match the experimental results well. High and low temperature zones can be seen depending on the design of the central pipe. Figure 4 shows the temperature profiles for design R_1 , which was considered a poor design in previous work due to the high flow at the last 15% of axial length due to the high flow resistance at the first 85% of the axial length [17]. High flow resistance in the bed relative to the central piping leads the hot gas to pass through the radial holes toward the outlet without depositing the energy in the storage materials, lowering energy storage in the bed. As can be seen, there is a decreasing temperature profile from $L=0-85$ cm followed by higher temperature from $L=85-100$ cm. The temperature from $L=0-85$ cm is not flat due to uneven flow distribution from the central pipe into the bed. The experimental temperature results in Figure 4b are averaged from three trials. As can be seen, small error bars confirm the repeatability of the experimental data.

Figure 5 shows the results for R_2 at two flow rates, where the hole size is varied in four segments along the length of the central pipe. Smaller holes toward the end of the bed and larger

holes near the inlet promote even flow and mitigate flow bypassing the packed bed. The increased resistance at the central pipe exit due to the smaller holes promotes uniform flow into the bed. More even flow into the bed leads to the flatter temperature profiles seen in the figure. The resulting flatter temperature profiles lead to more energy stored inside the packed bed domain and thus higher thermal efficiency [17] since all of the bed material is providing energy for storage. These results are explained in more detail in Section 3.2.

Note, an effect of using an average velocity in the heat transfer model is that local variations in the velocity are smoothed out in the averaging process. For example, consider the experimental results for design R₂ beyond the axial position of 0.6 m (Figure 5a). In the experiment in general, there is a rise in temperature from 0.6 to 0.8 m, and then a drop again toward the outlet. While the spread in temperature is not large, this

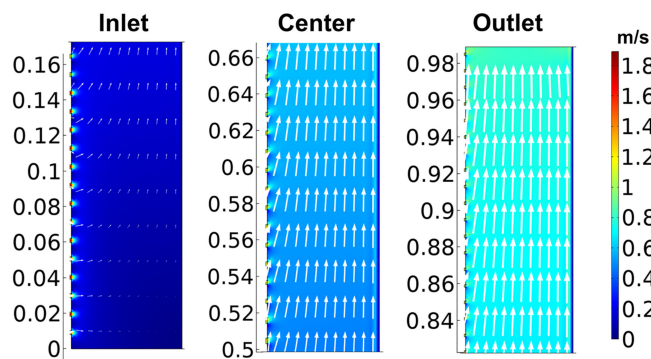


FIGURE 3 | Flow profiles for design R₂ at the inlet (~0–0.17 m), center (~0.5–0.67 m), and outlet regions (~0.83–1 m). Flow near the axial inlet shows predominantly radial flow. The flow rate decreases from inlet toward wall as expected in radial flow. At the axial center and outlet positions, flow is predominantly axial, with radial flow noted closer to the central pipe. At the outlet, the velocity vectors are largest as all flow exits via the packed bed outlet.

effect is not clearly captured by the model. A similar effect of averaging the velocity is seen in design R₁. The model does capture the decrease in temperature from 0 to 0.8 m and then a rise in temperature from 0.8 to 1 m; however, the magnitude of this effect is not captured by the model. Additionally, the discrete holes and random packing that occur in the experiment (captured schematically in Figure 1) lead to different experimental temperature values in the packed bed even at the same axial position along the bed. For instance, consider design R₂ at an axial position of ~0.7 m at 20 min of charging. There is a clear difference in temperature at this axial position despite the thermocouples being the same distance from the central pipe. While the model does not capture these experimental effects (caused by pore-scale heterogeneity in the system), the model result shows a temperature in between these values. Close agreement between profiles indicates that the model accurately captures the thermal energy transport in this system. As will be shown, the model and experiments lead to similar energetic efficiencies indicating similar amounts of energy stored in the bed. For 0.0061 m³/s, the same trends are observed, and the agreement between the model and experiment is good.

The strong agreement with experimental data also indicates that the flow profile in the heat transfer model successfully captures the effects one would see if considering the full pipe and all perforations (the flow-only model) at 0.0048 m³/s. These results are shown in Figure 6 at the packed bed exit. Compared with Figure 3, the maximum velocity from the center pipe into the bed is higher in the flow-only model (making the velocity vectors look relatively smaller). While this exact behavior is not captured in the heat transfer model due to the averaging process (explained above), this effect is only noted in the last ~5% of the axial length of the bed and the overall impact on thermal performance is small. One also sees the total velocity increase along the length of the bed as flow accumulates in the packing after exiting the central pipe. Thus,

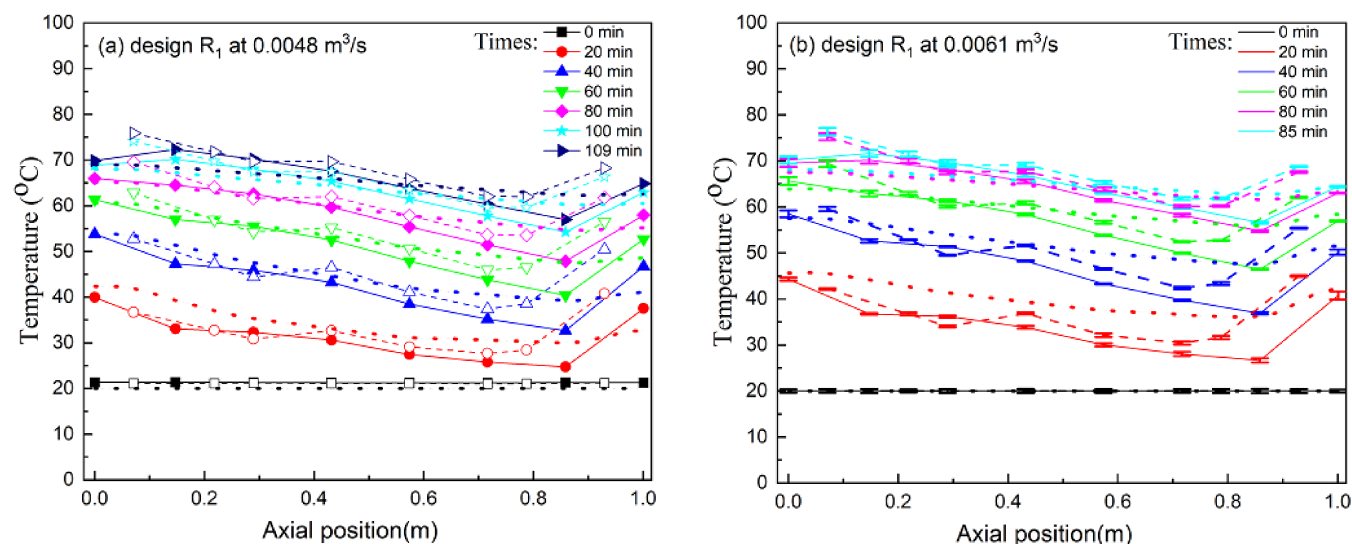


FIGURE 4 | Design R₁ with one fixed set of hole sizes in the central pipe spaced every 1 cm. The temperature distributions during the charging process are shown at two flow rates for (a) 0.0048 m³/s (from Reference [17]) and (b) 0.0061 m³/s. For the experimental results, 16 sensing points (solid lines for TC1 and dash lines for TC2) are plotted. Dotted lines indicate model results.

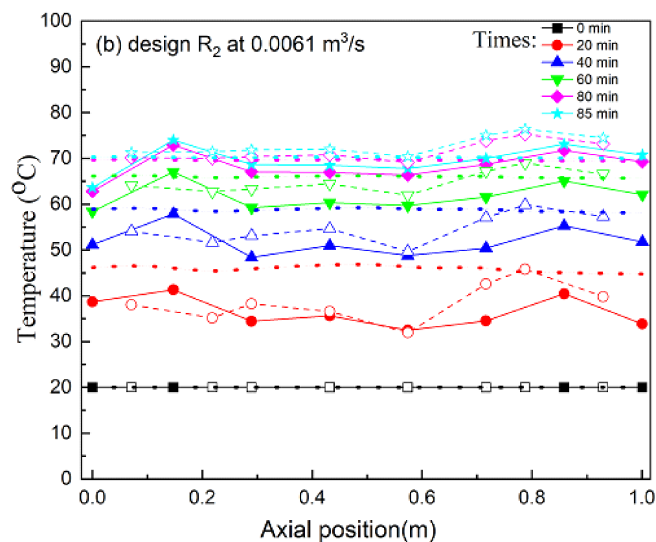
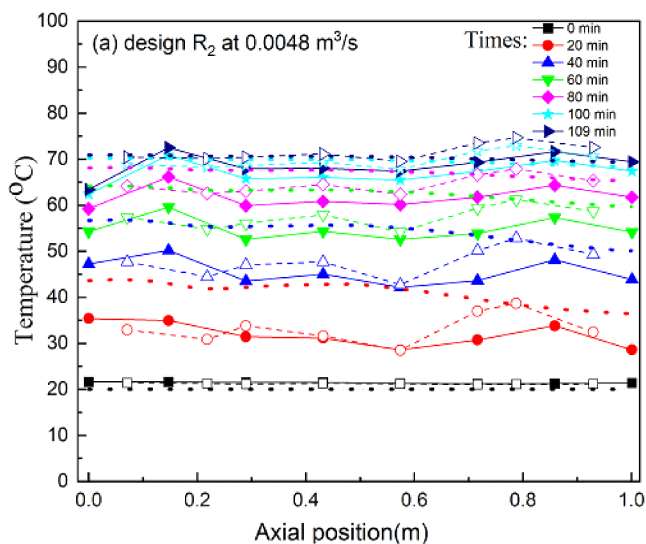


FIGURE 5 | Design R_2 with four layers that vary the hole sizes in the central pipe to promote even flow into the bed. Temperature distributions are shown during the charging process from the recent model and previous experimental data at two flow rates (a) $0.0048 \text{ m}^3/\text{s}$ (from Reference [17]) and (b) $0.0061 \text{ m}^3/\text{s}$. For the experiment data, 16 sensing points (solid lines for TC1 and dash lines for TC2) are plotted. Dotted lines indicate model results.

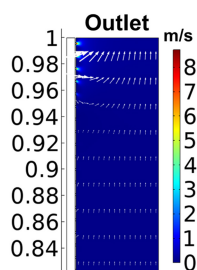


FIGURE 6 | Flow profile in the flow only model at steady state. Similar to the averaged velocity in the heat transfer model (Figure 3), flow near the axial outlet shows predominantly axial flow. The heat transfer model's velocity results show smaller spikes in magnitude due to the averaging process.

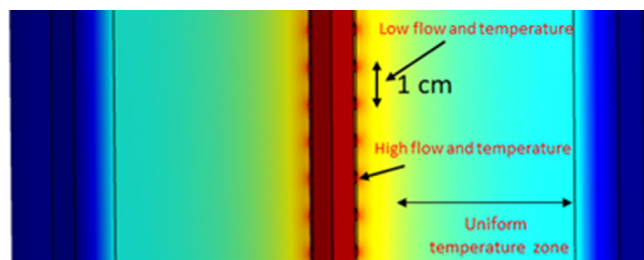


FIGURE 7 | 2-D axisymmetric temperature profile at 1200 s (20 min) during the charging process. Temperature fluctuations are visible close to the perforations due to flow exiting holes spaced at 1 cm intervals. A more uniform temperature profile is observed deeper in the packed bed away from the central pipe.

the combination of radial and axial flow is captured in the heat transfer model.

The results thus far have been at the same position as thermocouples from previous efforts. However, the shape of the temperature front in the radial direction is influenced by the hole design as well. As mentioned in the design section, the axial distance between each set of holes is 1 cm, providing zero flow through these solid sections. When the charging process starts, hot gas passes radially through the holes toward the bed wall. The temperature profiles just outside the central pipe look like a wave as a reflection of the flow through the radial pipe.

There are two reasons for the wavy behavior next to the central pipe, especially at early charging times: (1) flow through the radial holes is not 100% uniform and (2) hot gas will pass through the holes radially causing small 1 cm regions close to the radial pipe wall between the holes to not get enough hot gas at early times (e.g., 20 and 40 min). These results can be seen in Figure 7, where a 2-D surface plot shows the temperature distribution (20 min) in all domains at $0.0048 \text{ m}^3/\text{s}$. As can be

observed, at the outlet of the holes the temperature is high, while between the holes the temperature is lower. The wavy temperature profiles disappear by moving into the packed bed toward the wall bed.

3.2 | Thermal Performance: Charging Efficiency

Figure 8 shows the temperature profile of the full bed at different time steps during the charging process for design R_1 , design R_2 , and a traditional axial bed operating at the same temperature and flow conditions at $0.0048 \text{ m}^3/\text{s}$. As can be noticed, the entire bed for design R_2 is at higher temperatures at the end of charging compared with the design R_1 and the axial flow configuration, leading to higher energy storage and thus higher charging efficiency. Important differences emerge between designs R_1 and R_2 , which are reflective of the flow results discussed above. For R_1 , at the early and medium charging times, one sees higher temperature near the central pipe at the outlet, consistent with bypass flow. The bypass means energy enters the system but is not deposited in the bed. Design R_2 shows much more uniform temperature

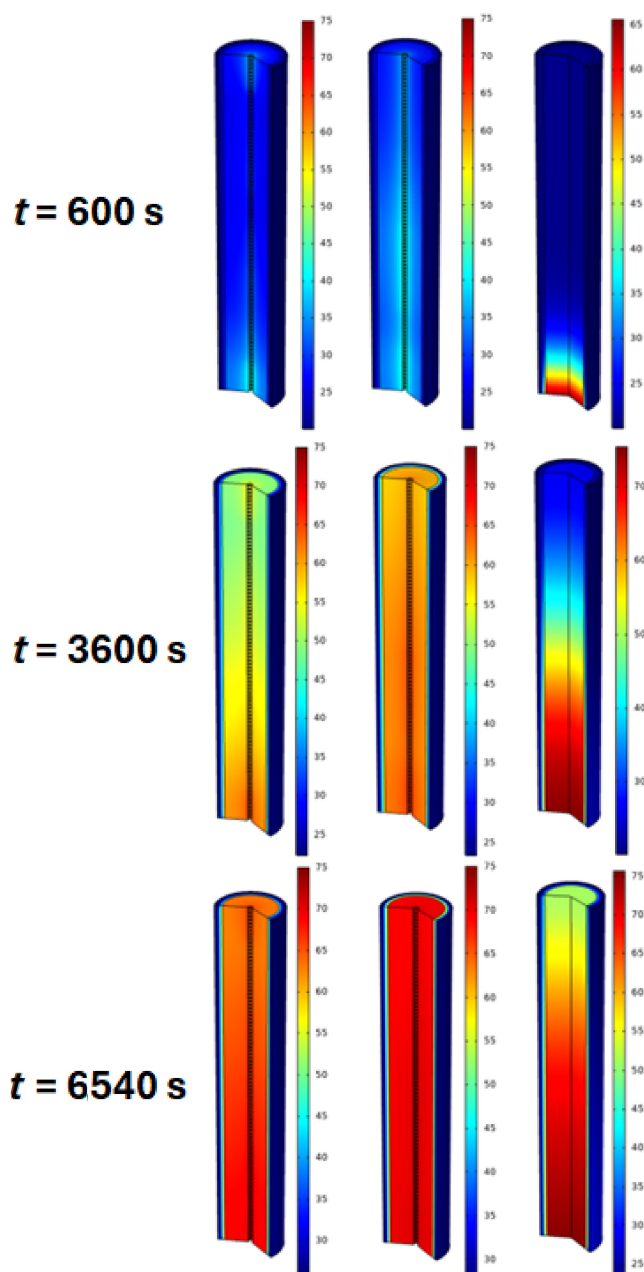


FIGURE 8 | Temperature distribution during charging at three different time steps (600, 3600, and 6540 s) for the HRA configurations and traditional axial flow configuration. HRA R_1 = Left. HRA R_2 = Center. Axial = Right. The results clearly show the flow configuration affects the temperature distribution in the bed. HRA R_2 shows higher and more uniform temperature compared with HRA R_1 .

distributions along the axial length, consistent with more uniform flow entering the bed from the central pipe. In each hybrid case, the temperature gradient in the radial direction is minimal due to the axial flow that emerges after radial introduction. Thus, the HRA thermocline is distinct when compared with axial or purely radial TES. The axial configuration performs as expected with a clear thermocline dividing the hot and cold zones of the bed along the axial length.

The total energy was calculated by volume averaging the bed domain temperature at each time point during the charging process.

The energy over time for the radial and classical axial configurations at two flow rates are shown in Figure 9a,b. For a flow rate of $0.0048 \text{ m}^3/\text{s}$, the final total energy is 1035.9, 1099.7, and 1071.5 kJ for HRA design R_1 , HRA design R_2 , and axial flow, respectively. For flow of $0.0061 \text{ m}^3/\text{s}$, the total energy calculated from the model is 1007.2, 1128.9, and 1096.7 kJ for HRA design R_1 , HRA design R_2 , and axial flow, respectively. Dividing the total energy delivered by the HTF over that time yields thermal energy efficiency.

Table 3 shows the resulting charging efficiency for the HRA designs and axial flow based on the first law of thermodynamics, which is adopted from [17]. The charging efficiency from the model agrees with the experimental charging efficiency for the hybrid flow designs, R_1 and R_2 , and for traditional axial flow at the same temperature and flow rate. As can be seen, the numerical charging efficiency for HRA design R_2 is better than the charging efficiency for traditional axial flow, which is consistent with experimental results. HRA design R_1 shows the lowest performance due to heated flow bypassing the packed bed, as shown by the model results here. The bypass leads to heating near the outlet, which can also be seen in the early and medium time results of Figure 8 for design R_1 .

Published studies that used radial flow as charging or discharging configuration [5, 7–15] all considered fluid moving from the center to the wall or from the wall to the center with no axial flow within the packed bed. As stated in the introduction, the present pipe injection scheme used in the present work is a novel scheme, where flow in the bed domain is radial and axial. In addition, the present study focuses on the flat temperature profiles inside the bed domain, which is a function of the design of the central pipe, to determine the thermal performance and thus the thermal charging efficiency. Even flow distribution enhances the flat temperature profiles inside the bed domain, which leads to more stored energy. Therefore, the pipe injection method is different than the classical TES systems (the axial flow systems) and the previous radial flow studies.

4 | Conclusion

The thermal performance in a packed bed TES system is analyzed numerically via charging the bed domain in a new HRA configuration. In the hybrid system, the HTF exits a central perforated pipe during charge, and then flows through the packed bed toward the packed bed's axial exit. Radial and axial velocity is noted in the bed depending on the spatial location, hence referring to the system as HRA. Two CFD models were utilized. A flow only model considered flow in the central pipe, through the perforations, and through the packed bed. The average velocity of the fluid exiting the central holes was applied in a heat transfer model to calculate the temperature profile in the packed bed. Alumina spheres at 6 mm and air at 75°C were used as storage materials and HTF for comparison to previously published experimental data. Two central pipe designs were considered in the HRA configuration, and the numerical results match the experimental results reasonably well. Design R_1 was based on a constant hole design through the central pipe, while design R_2 used diminishing holes sizes along the length of the central pipe to promote even flow into the packing. In summary:

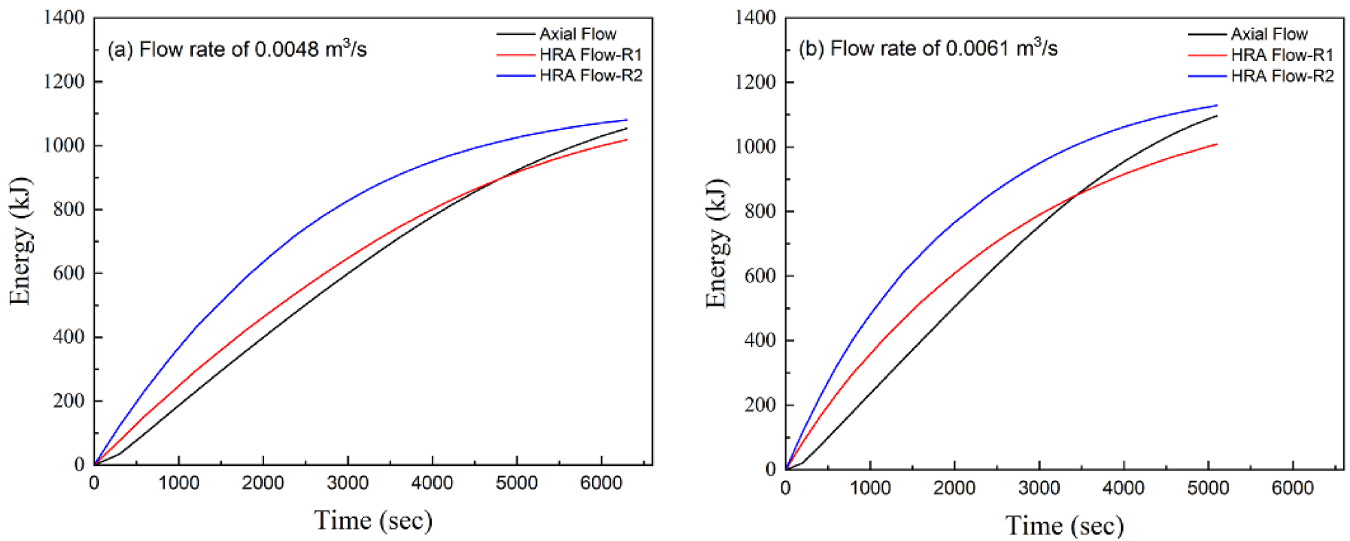


FIGURE 9 | Thermal energy stored in the bed over time for HRA: HRA R_1 , HRA R_2 , and traditional axial flow. More energy is stored with HRA R_2 , indicated the HRA approach to TES can be more efficient in charging if the central pipe is correctly designed.

TABLE 3 | Percentage charging efficiency from the model and experimental results for HRA and traditional axial flow.

Flow configuration	Charging efficiency (%)			
	0.0048 m ³ /s		0.0061 m ³ /s	
	Experimental	Model	Experimental	Model
HRA design R_1	71.5	71.7	72.9 ± 0.7	71.2
HRA design R_2	77.8	75.5	81.9	80.5
Traditional axial	75.3	73.8	77.7	78.1

Note: Experimental results for 0.0048 m³/s are from Reference [17].

- In the HRA approach, the hot air passes through the central pipe's holes radially and then leaves the bed axially. Radial flow behavior is very clear toward the inlet of the packed bed. Then, the mass flow accumulates toward the exit of the bed, leading to approximately 100% axial flow at the outlet of the storage packed bed.
- The energy stored and thus charging efficiency in the HRA flow for design R_2 is better than that of classical axial flow. Design R_2 is better than R_1 due to the division of the radial pipe length into four layers, where each layer has different holes sizes to promote even flow into the bed. For 0.0048 m³/s, the charging efficiencies are 71.7% for R_1 and 75.5% for R_2 from the model, respectively, which match the experimental data. The charging efficiency for a traditional axial flow model at the same conditions is 73.8%. For 0.0061 m³/s, the charging efficiencies are 71.2% for R_1 and 80.5% for R_2 based on the model results. The charging efficiency for a traditional axial flow model at this higher flow rate and same conditions is 78.1%. These results indicate that the thermal efficiency can be higher with HRA flow compared with axial flow when the central pipe is correctly designed. Future research will assess charge/discharge cycles and thermal exergy efficiency at high temperatures.

Nomenclature

β	inertial term in packed bed pressure drop
K	viscous term in packed bed pressure drop
μ	gas viscosity (Pa s)
ζ	efficiency (-)
ϵ	packed bed porosity (-)
u	velocity vector (m/s)
ρ	density (kg/m ³)
p	pressure (Pa)
C_p	specific heat capacity (J/kg K)
L	length (height) of packed bed (m)
k	thermal conductivity (W/m K)
\dot{m}	mass flow rate (kg/s)
Q_{loss}	energy losses to surrounding (W/m ³)
t	time (s)
T	temperature (K)

Subscripts

s	solid
f	fluid
0	initial
eff	effective
i	solid domains (steel and insulation)

Acknowledgments

This research did not receive any specific grant from funding agencies in the public, commercial, or not-for-profit sectors. R.A. thanks Montana State University for funding the COMSOL modules.

Conflicts of Interest

The authors declare no conflicts of interest.

Data Availability Statement

The data that support the findings of this study are available from the corresponding author upon reasonable request.

References

1. A. Palacios, C. Barreneche, M. Navarro, and Y. Ding, "Thermal Energy Storage Technologies for Concentrated Solar Power—A Review From a Materials Perspective," *Renewable Energy* 156 (2020): 1244–1265.
2. G. Manente, Y. Ding, and A. Sciacovelli, "A Structured Procedure for the Selection of Thermal Energy Storage Options for Utilization and Conversion of Industrial Waste Heat," *Journal of Energy Storage* 51 (2022): 104411.
3. A. Gautam and R. Saini, "A Review on Technical, Applications and Economic Aspect of Packed Bed Solar Thermal Energy Storage System," *Journal of Energy Storage* 27 (2020): 101046.
4. T. Esence, A. Bruch, S. Molina, B. Stutz, and J. F. Fourmigué, "A Review on Experience Feedback and Numerical Modeling of Packed-Bed Thermal Energy Storage Systems," *Solar Energy* 153 (2017): 628–654.
5. S. Trevisan, W. Wang, R. Guedez, and B. Laumert, "Experimental Evaluation of a High-Temperature Radial-Flow Packed Bed Thermal Energy Storage Under Dynamic Mass Flow Rate," *Journal of Energy Storage* 54 (2022): 105236.
6. T. M. Sanderson and G. T. Cunningham, "Packed Bed Thermal Storage Systems," *Applied Energy* 51, no. 1 (1995): 51–67.
7. J. D. McTigue and A. J. White, "A Comparison of Radial-Flow and Axial-Flow Packed Beds for Thermal Energy Storage," *Applied Energy* 227, no. C (2018): 533–541.
8. S. Trevisan, R. Guédez, H. Bouzekri, and B. Laumert, "Initial Design of a Radial-Flow High Temperature Thermal Energy Storage Concept for Air-Driven CSP Systems," in *AIP Conference Proceedings* (Melville, NY: AIP Publishing LLC, 2019).
9. S. Trevisan, W. Wang, R. Guedez, and B. Laumert, "Experimental Evaluation of an Innovative Radial-Flow High-Temperature Packed Bed Thermal Energy Storage," *Applied Energy* 311 (2022): 118672.
10. S. Trevisan, W. Wang, R. Guédez, and B. Laumert, "Laboratory Prototype of an Innovative Radial Flow Packed Bed Thermal Energy Storage," in *AIP Conference Proceedings* (Melville, NY: AIP Publishing, 2022).
11. W. H. Gerstle, N. R. Schroeder, L. P. McLaughlin, C. K. Ho, H. F. Laubscher, and S. Kao, "Experimental Testing and Computational Modeling of a Radial Packed Bed for Thermal Energy Storage," *Solar Energy* 264 (2023): 111993.
12. C. K. Ho and W. Gerstle, "Terrestrial Heat Repository for Months of Storage (THERMS): A Novel Radial Thermocline System," in *Energy Sustainability* (New York, NY: American Society of Mechanical Engineers, 2021).
13. M. E. Skuntz, R. Elander, M. Al-Azawii, P. Bueno, and R. Anderson, "System Efficiency of Packed Bed TES With Radial Flow vs. Axial Flow—Influence of Aspect Ratio," *Journal of Energy Storage* 72 (2023): 108463.
14. R. Anderson, B. B. Yayalar, M. Al-Azawii, R. Elander, M. E. Skuntz, and P. Bueno, "Radial Flow Packed Beds With Internal Segmentation for Thermal Energy Storage," in *ASTFE Digital Library* (Danbury, CT: Begell House Inc, 2024): 06810.
15. D. M. Beck, M. Al-Azawii, P. C. Bueno, and R. Anderson, "Enhancing Even Gas Distribution in Porous Media With Radial Flow," in *AIAA SCITECH 2022 Forum* (Reston, VA: AIAA Press, 2022).
16. T. Wu, D. Wang, R. Wang, et al., "Pressure Drop Axial Distribution Uniformity of the Particle Bed in the Radial Bed," *Korean Journal of Chemical Engineering* 38, no. 8 (2021): 1578–1591.
17. M. M. Al-Azawii, D. Jacobsen, P. Bueno, and R. Anderson, "Experimental Study of Thermal Behavior During Charging in a Thermal Energy Storage Packed Bed Using Radial Pipe Injection," *Applied Thermal Engineering* 180 (2020): 115804.
18. D. A. Nield and A. Bejan, *Convection in Porous Media*, vol. 3 (New York, NY: Springer, 2013).
19. M. M. S. Al-Azawii, C. Theade, P. Bueno, and R. Anderson, "Experimental Study of Layered Thermal Energy Storage in an Air-Alumina Packed Bed Using Axial Pipe Injections," *Applied Energy* 249 (2019): 409–422.
20. M. M. S. Al-Azawii, C. Theade, M. Danczyk, E. Johnson, and R. Anderson, "Experimental Study on the Cyclic Behavior of Thermal Energy Storage in an Air-Alumina Packed Bed," *Journal of Energy Storage* 18C (2018): 239–249.
21. R. Anderson, L. Bates, E. Johnson, and J. F. Morris, "Packed Bed Thermal Energy Storage: A Simplified Experimentally Validated Model," *Journal of Energy Storage* 4 (2015): 14–23.
22. D. Vortmeyer and R. Schaefer, "Equivalence of One- and Two-Phase Models for Heat Transfer Processes in Packed Beds: One Dimensional Theory," *Chemical Engineering Science* 29, no. 2 (1974): 485–491.
23. A. Bejan and A. D. Kraus, *Heat Transfer Handbook* (Hoboken, NJ: John Wiley & Sons, INC, 2003).
24. F. P. Incropera, *Fundamentals of Heat and Mass Transfer*, 6th ed., eds. F. P. Incropera, D. P. DeWitt, T. L. Bergman, and A. S. Lavine (Hoboken, NJ: John Wiley, 2007).